Optimized Protocols for Duplex Quantum Transduction

Zhaoyou Wang,* Mengzhen Zhang, Yat Wong, Changchun Zhong, and Liang Jiang†
Pritzker School of Molecular Engineering, University of Chicago, Chicago, Illinois 60637, USA

(Received 8 July 2023; accepted 25 October 2023; published 30 November 2023)

Quantum transducers convert quantum signals through hybrid interfaces of physical platforms in quantum networks. Modeled as quantum communication channels, performance of unidirectional quantum transduction can be measured by the quantum channel capacity. However, characterizing performance of quantum transducers used for duplex quantum transduction where signals are converted bidirectionally remains an open question. Here, we propose rate regions to characterize the performance of duplex quantum transduction. Using this tool, we find that quantum transducers optimized for simultaneous duplex transduction can outperform strategies based on the standard protocol of time-shared unidirectional transduction. Integrated over the frequency domain, we demonstrate that the rate region can also characterize quantum transducers with finite bandwidth.

DOI: 10.1103/PhysRevLett.131.220802

Introduction.—Quantum transducers convert quantum signals between physically distinct carriers, enabling quantum information exchange across multiple platforms in quantum networks [1]. For example, a microwave-to-optical quantum transducer [2–13] can distribute processed quantum states stored in superconducting qubits over optical fibers. Various designs of quantum transducers have been developed, utilizing hybrid interfaces like electro-optics [6,7,10,11,14], optomechanics [4,5,8,9,13,15–20], and electromagnonics [13,21,22].

As devices for quantum state transfer, quantum transducers can be abstracted as quantum channels. Most bosonic quantum transducers use red-detuned pumps [3,4,6–10] to engineer a two-mode scattering process that is equivalent to a beam splitter. The input signal of one mode $\hat{a}_{1,\mathrm{in}}(\hat{a}_{2,\mathrm{in}})$ gets converted to the output signal of the other mode $\hat{a}_{2,\mathrm{out}}(\hat{a}_{1,\mathrm{out}})$, yielding two unidirectional transduction channels $\mathcal{E}_1$ and $\mathcal{E}_2$ [Fig. 1(a)]. Oftentimes, only a single channel is utilized to transduce the quantum signal from one mode to the other, which we refer to as *unidirectional* quantum transduction. The performance of unidirectional quantum transduction is characterized by the quantum capacity of either $\mathcal{E}_1$ or $\mathcal{E}_2$ [23,24].

By leveraging both unidirectional transduction channels, quantum signals can be converted bidirectionally which we refer to as *duplex* quantum transduction [25]. Duplex quantum transduction can be modeled as a quantum interference channel [26–28], with senders $A(\hat{a}_{1,\mathrm{in}})$ and $B(\hat{a}_{2,\mathrm{in}})$ and receivers $C(\hat{a}_{2,\mathrm{out}})$ and $D(\hat{a}_{1,\mathrm{out}})$. The senders and receivers can be distinct users by separating the input and output signals of each mode with circulators [Fig. 1(b)]. For example, a lossless beam splitter with efficiency T [Fig. 1(c)] implements a quantum interference channel:

$$\begin{aligned}\mathcal{E}_{1,A\to D}&:\ \hat{a}_{2,\mathrm{out}}=\sqrt{T}\hat{a}_{1,\mathrm{in}}+\sqrt{1-T}\hat{a}_{2,\mathrm{in}},\\ \mathcal{E}_{2,B\to C}&:\ \hat{a}_{1,\mathrm{out}}=\sqrt{T}\hat{a}_{2,\mathrm{in}}-\sqrt{1-T}\hat{a}_{1,\mathrm{in}}.\end{aligned}\tag{1}$$

One strategy for duplex quantum transduction is to alternate between using $\mathcal{E}_1$ and $\mathcal{E}_2$, while simultaneous transduction of uncorrelated input signals $\hat{a}_{1,\mathrm{in}}$ and $\hat{a}_{2,\mathrm{in}}$ may be more efficient. However, $\mathcal{E}_1$ and $\mathcal{E}_2$ can interfere with each other when put in use simultaneously, e.g., the input signal $\hat{a}_{1,\mathrm{in}}$ for $\mathcal{E}_1$ acts as added noise for $\mathcal{E}_2$ in a beam splitter [Eq. (1)]. As a result, characterizing the performance of duplex quantum transduction requires a new metric beyond the quantum capacities of the individual unidirectional transduction channels.

We propose to use the achievable information rate region as the performance metric. The achievable rates of a quantum device depend on the quantum channels it implements as well as the input signal encodings, with channel parameters [such as T in Eq. (1)] determined by the physical device parameters. In duplex quantum transduction, both transduction channels $\mathcal{E}_1$ and $\mathcal{E}_2$ transmit quantum information at rates I_1 and I_2, respectively. For *simultaneous* duplex transduction, the pair of achievable rates (I_1, I_2) depends on how we encode quantum information into quantum signals. By varying the encodings for $\hat{a}_{1,\mathrm{in}}$ and $\hat{a}_{2,\mathrm{in}}$, we obtain a two-dimensional region of achievable information rates $\{(I_1, I_2)\}$ [Fig. 1(d)]. The rate region characterizes the performance of simultaneous duplex transduction and its boundary indicates the optimized coding strategies. Past studies have also employed rate regions or capacity regions to study the trade-off among multiple quantum channels, albeit limited to sending classical information [26,27,29–31] or distributing

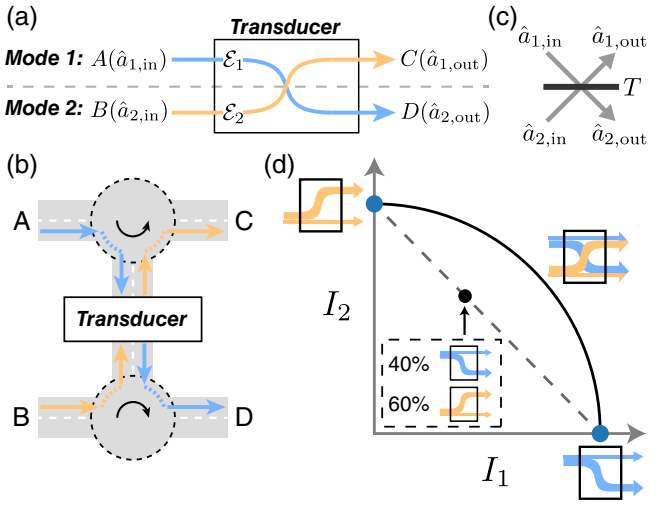

FIG. 1. (a) Quantum signals converted from one mode to the other with a quantum transducer, where $\mathcal{E}_1$ and $\mathcal{E}_2$ are the unidirectional transduction channels. (b) Separating the input and output signals of each mode with circulators. (c) Beam splitter with efficiency T. (d) Schematic of the rate region (black line) for duplex quantum transduction. Blue dots: quantum capacity of the unidirectional transduction channels. Gray dashed line: achievable rates for the time-shared unidirectional transduction.

entanglement in qubit-based quantum networks [32–35]. So far, there is no analysis investigating the achievable quantum information rate region at the hardware level, such as quantum transducers.

Furthermore, we can combine simultaneous duplex transduction with the *time-sharing* strategy, where we alternate between different signal encodings and even device parameters. This leads to a new region of achievable rates that is the convex hull of the original region, and we refer to the new region as the time-sharing achievable rate region. For example, we can perform transduction in one direction with $\mathcal{E}_1$ for 40% of the time and in the opposite direction with $\mathcal{E}_2$ for the remaining 60% of the time [black dot, Fig. 1(d)]. Notably, when the original region is not convex, time-sharing can offer an additional performance boost for duplex quantum transduction.

In this Letter, we define the (time-sharing) achievable rate region and apply the tool to characterize the performance of two-mode quantum transducers. We demonstrate that a sizable portion of quantum transducers can benefit from simultaneously transducing quantum signals in both directions. We also discuss how reflectionless scattering leads to the optimal duplex quantum transduction, as well as the effect of finite bandwidth.

Rate regions of duplex quantum transduction.—We consider quantum transducers with a linear input-output relation

$$\begin{pmatrix} \hat{a}_{1,\mathrm{out}} \\ \hat{a}_{2,\mathrm{out}} \\ \vdots \\ \hat{a}_{n,\mathrm{out}} \end{pmatrix} = S \begin{pmatrix} \hat{a}_{1,\mathrm{in}} \\ \hat{a}_{2,\mathrm{in}} \\ \vdots \\ \hat{a}_{n,\mathrm{in}} \end{pmatrix}, \tag{2}$$

where the scattering matrix S is unitary and depends on the device parameters of the transducer [3]. We choose ports 1 and 2 as the signal ports, and $\hat{a}_{n>2,\mathrm{in}}$ are the injected vacuum noise from the internal loss channels. The two transduction channels are

$$\begin{aligned} &\mathcal{E}_{1,A\to D}\colon\ \hat{a}_{2,\mathrm{out}} = S_{21}\hat{a}_{1,\mathrm{in}} + S_{22}\hat{a}_{2,\mathrm{in}} + \sum_{n>2} S_{2n}\hat{a}_{n,\mathrm{in}}, \\ &\mathcal{E}_{2,B\to C}\colon\ \hat{a}_{1,\mathrm{out}} = S_{12}\hat{a}_{2,\mathrm{in}} + S_{11}\hat{a}_{1,\mathrm{in}} + \sum_{n>2} S_{1n}\hat{a}_{n,\mathrm{in}}. \end{aligned} \tag{3}$$

Intuitively, the transmission coefficients S_{12} and S_{21} determine the transduction efficiency, while the reflection coefficients S_{11} and S_{22} lead to the interference between $\mathcal{E}_1$ and $\mathcal{E}_2$.

Here we define the achievable information rates for simultaneous duplex transduction. For a quantum channel $\mathcal{E}\colon \mathcal{L}(\mathcal{H}) \to \mathcal{L}(\mathcal{H})$, the achievable rate of quantum information with an input state $\hat{\rho}$ is measured by the coherent information $I(\mathcal{E},\hat{\rho})$ [36]. Let $|\psi\rangle \in \mathcal{H}\otimes\mathcal{H}'$ be a purification of $\hat{\rho}$; we have

$$I(\mathcal{E},\hat{\rho}) \equiv H[\mathcal{E}(\hat{\rho})] - H[(\mathcal{E}\otimes\mathcal{I}')(|\psi\rangle\langle\psi|)], \tag{4}$$

where $H(\hat{\rho})$ is the von Neumann entropy of $\hat{\rho}$ and $\mathcal{I}'$ is the identity map on $\mathcal{H}'$. For $I(\mathcal{E},\hat{\rho}) < 0$, the achievable rate is 0. Generalizing to a quantum interference channel $\mathcal{E}_{(A,B)\to(C,D)}\colon \mathcal{L}(\mathcal{H}_1\otimes\mathcal{H}_2) \to \mathcal{L}(\mathcal{H}_1\otimes\mathcal{H}_2)$, the simultaneously achievable information rates (I_1, I_2) with uncorrelated input state $\hat{\rho}_1\otimes\hat{\rho}_2$ are

$$\begin{aligned} &I_1(\mathcal{E},\hat{\rho}_1\otimes\hat{\rho}_2) \equiv I(\mathcal{E}_1,\hat{\rho}_1), \qquad \mathcal{E}_1(\cdot) = \mathrm{Tr}_1\mathcal{E}(\cdot,\hat{\rho}_2), \\ &I_2(\mathcal{E},\hat{\rho}_1\otimes\hat{\rho}_2) \equiv I(\mathcal{E}_2,\hat{\rho}_2), \qquad \mathcal{E}_2(\cdot) = \mathrm{Tr}_2\mathcal{E}(\hat{\rho}_1,\cdot). \end{aligned} \tag{5}$$

Given the challenges in determining the quantum capacity for lossy channels with added noise [37–40], we focus on the rate region achievable with thermal input states as a lower bound. When the input signals of $\mathcal{E}_1$ and $\mathcal{E}_2$ are thermal states with average photon number N_1 and N_2, the outputs are also thermal states with photon number $N_1' = TN_1 + R_2N_2$ and $N_2' = TN_2 + R_1N_1$ [Fig. 2(a)]. Here $R_i = |S_{ii}|^2$ is the power reflection coefficient from port i, $T_{ij} = |S_{ij}|^2$ is the power transmission coefficient from port j to port i, and we assume $T_{12} = T_{21} \equiv T$. For finite R_1 and R_2, the reflected signal from one channel adds thermal noise to the other channel, which leads to the tradeoff between I_1 and I_2 for simultaneous duplex transduction.

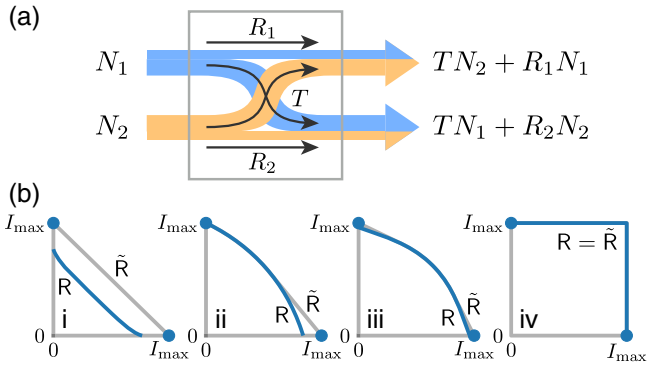

FIG. 2. (a) Duplex transduction with thermal input states. (b) The rate regions (blue dot and lines) and time-sharing rate regions (gray lines) at $T = 0.9$ for different reflection coefficients $(R_1, R_2) = (0.03, 0.03), (0.03, 0), (0.003, 0.003), (0, 0)$.

The achievable rates (I_1, I_2) for Eq. (3) with thermal input states (N_1, N_2) are (see Supplemental Material (SM) [41])

$$I_k(T, R_1, R_2, N_1, N_2) = h(N'_k) - h\left(\frac{D_k + N'_k - N_k - 1}{2}\right) - h\left(\frac{D_k - N'_k + N_k - 1}{2}\right), \quad (6)$$

where $k = 1, 2$,

$$h(x) = (x+1)\log_2(x+1) - x\log_2(x), \quad (7)$$

and

$$D_k = \sqrt{(N_k + N'_k + 1)^2 - 4TN_k(N_k + 1)}. \quad (8)$$

The rate region $\mathsf{R} \equiv \{(I_1, I_2) | \forall (N_1, N_2)\}$ only depends on channel parameters (T, R_1, R_2). We could combine simultaneous duplex transduction with the time-sharing protocol, and the resulting time-sharing rate region is the convex hull $\tilde{\mathsf{R}} = \mathrm{Conv}(\mathsf{R})$. Additionally, numerical evidence suggests that thermal encodings are likely optimal among general Gaussian encodings (see SM [41]). The rate regions can be calculated similarly when the environment injects thermal noise rather than vacuum noise via the internal loss channels $\hat{a}_{n>2,\mathrm{in}}$ (see SM [41]).

The rate region R can be determined from its boundary $\partial\mathsf{R}$. For the special cases of unidirectional quantum transduction with $(N_1, N_2) = (\infty, 0)$ and $(0, \infty)$, we achieve information rates $(I_{\max}, 0)$ and $(0, I_{\max})$ on $\partial\mathsf{R}$ [Fig. 2(b), blue dots]. Here $I_{\max} = \max\{\log_2(T/(1-T)), 0\}$ is the quantum capacity of the pure-loss channel [48]. For $I_1 > 0$ and $I_2 > 0$, R corresponds to a continuous mapping $(N_1, N_2) \to (I_1, I_2)$ and $\partial\mathsf{R}$ can be solved numerically with the low-rank Jacobian condition $\det(J) = 0$, where J is the 2×2 Jacobian matrix. In Fig. 2(b), we plot the rate regions R (blue lines and dots) and $\tilde{\mathsf{R}}$ (gray lines) for different reflection coefficients (R_1, R_2). We choose $T = 0.9$ with $I_{\max} \approx 3.17$.

Finite reflection R_k results in a noticeable discontinuity of the boundary $\partial\mathsf{R}$ at the I_k axis [Figs. 2(b)i–2(b)iii]. This can be explained from the upper bound on the thermal-loss capacity [49–51]. Assuming $R_1 > 0$, the channel $\mathcal{E}_{2,B\to C}$ is a thermal loss channel with noise photon $\bar{N} = R_1N_1/(1-T)$. From the upper bound [49–51]

$$I_2 \le \max\left\{\log_2\left[\frac{T - (1-T)\bar{N}}{(1-T)(\bar{N}+1)}\right], 0\right\}, \quad (9)$$

we must have $N_1 < (2T-1)/2R_1$ to achieve a positive information rate $I_2 > 0$. On the other hand, when $I_2 = 0$ the quantum capacity $I_1 = I_{\max}$ is achieved at $N_1 \to \infty$, which leads to the discontinuity at $I_2 = 0$.

If one side is reflectionless with $R_k = 0$, the discontinuity of $\partial\mathsf{R}$ vanishes at the I_k axis [Fig. 2(b)ii I_2 axis]. If both sides are reflectionless, there is no interference between the two transduction channels and the maximal square region can be achieved [Fig. 2(b)iv]. Therefore it is possible to outperform the time-shared unidirectional transduction [Fig. 1(d) gray dashed line] with the simultaneous duplex transduction, as long as the reflection coefficients are small [Figs. 2(b)ii–2(b)iv].

So far we have only considered direct transduction without adaptive control [23] or shared entanglement [52–54]. In the SM [41], we briefly discuss duplex quantum transduction assisted with local operations and classical communication, along with the scenario where the senders are the same as the receivers which allows one to use the interference-based techniques [55,56].

Optimized transduction protocols.—Here we apply the tool of rate regions to analyze a physical transducer model. The channel parameters (T, R_1, R_2), and thus the achievable rates, depend on the device parameters of the transducer. We therefore generalize the achievable rate regions to include not only different signal encodings but also different device parameters. The boundary of the resulting rate region leads to optimized signal encodings and device parameters for the transducer.

We consider a transducer model for frequency conversion between two bosonic modes $\hat{a}_1$ and $\hat{a}_2$ [Fig. 3(a)]. The lab frame Hamiltonian is

$$\hat{H} = \omega_1\hat{a}_1^\dagger\hat{a}_1 + \omega_2\hat{a}_2^\dagger\hat{a}_2 + g\left(\hat{a}_1^\dagger\hat{a}_2 e^{i\omega_p t} + \hat{a}_1\hat{a}_2^\dagger e^{-i\omega_p t}\right), \quad (10)$$

where ω_k are the mode frequencies, ω_p is the pump frequency and g is the interaction rate. An input signal at frequency ω in mode 1 gets converted to an output signal at frequency $\omega + \omega_p$ in mode 2, and vice versa. The Hamiltonian in the rotating frame of the signal is

$$\hat{H} = \Delta_1\hat{a}_1^\dagger\hat{a}_1 + \Delta_2\hat{a}_2^\dagger\hat{a}_2 + g\left(\hat{a}_1^\dagger\hat{a}_2 + \hat{a}_1\hat{a}_2^\dagger\right), \quad (11)$$

where $\Delta_1 = \omega_1 - \omega$ and $\Delta_2 = \omega_2 - \omega_p - \omega$.

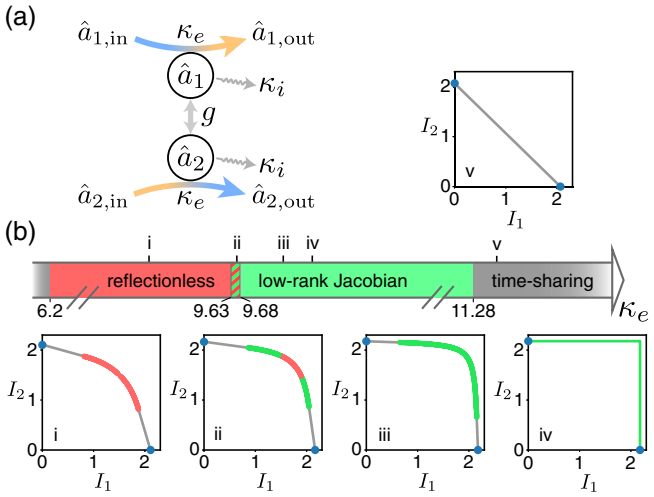

FIG. 3. (a) Schematic of a physical transducer model. (b) Optimized protocols achieving the boundary $\partial\tilde{\mathsf{R}}$ for the time-shared duplex transduction at different κ_e. Here i–v correspond to $\kappa_e = 9.2, 9.66, 9.9, 10.05, 11.4$, respectively.

Assuming mode k has external (internal) loss rate $\kappa_{k,e(i)}, k = 1, 2$, the scattering matrix only depends on the ratios $\kappa_{k,e}/\kappa_{k,i}$ (see SM [41]). In practice, the loss rates of two modes may differ by orders of magnitude, but the ratios $\kappa_{1,e}/\kappa_{1,i}$ and $\kappa_{2,e}/\kappa_{2,i}$ are often close [6,10,11]. Therefore, we assume symmetric loss rates $\kappa_{1,e(i)} = \kappa_{2,e(i)} \equiv \kappa_{e(i)}$ for simplicity and the more general case is discussed in the SM [41]. The input-output relation is given by

$$\begin{pmatrix} \hat{a}_{1,\mathrm{out}} \\ \hat{a}_{2,\mathrm{out}} \\ \tilde{a}_{1,\mathrm{out}} \\ \tilde{a}_{2,\mathrm{out}} \end{pmatrix} = S \begin{pmatrix} \hat{a}_{1,\mathrm{in}} \\ \hat{a}_{2,\mathrm{in}} \\ \tilde{a}_{1,\mathrm{in}} \\ \tilde{a}_{2,\mathrm{in}} \end{pmatrix}, \tag{12}$$

where $\tilde{a}_{k,\mathrm{in(out)}}$ are the internal loss channels, and

$$S = \begin{pmatrix} I + \kappa_e M & \sqrt{\kappa_e \kappa_i} M \\ \sqrt{\kappa_e \kappa_i} M & I + \sqrt{\kappa_i} M \end{pmatrix}. \tag{13}$$

Here I is the 2×2 identity matrix, and

$$M = -\left(iG + \frac{\kappa_e + \kappa_i}{2} I \right)^{-1}, \qquad G = \begin{pmatrix} \Delta_1 & g \\ g & \Delta_2 \end{pmatrix}. \tag{14}$$

We focus on optimizing the detunings (Δ_1, Δ_2) of the transducer, while keeping other relevant parameters (g, κ_e, κ_i) fixed. Besides the signal encodings (N_1, N_2), the achievable rates (I_1, I_2) also depend on the device parameters $(\Delta_1, \Delta_2, g, \kappa_e, \kappa_i)$. We therefore define the rate region as $\mathsf{R} \equiv \{(I_1, I_2) | \ \forall\ (N_1, N_2, \Delta_1, \Delta_2)\}$. The optimized signal encodings (N_1, N_2) and detunings (Δ_1, Δ_2) can be obtained from the boundary $\partial\tilde{\mathsf{R}}$ of the time-sharing rate region $\tilde{\mathsf{R}}$.

The boundary of the rate region can be determined by exploring several possible solutions. On the I_1 and I_2 axes, the quantum capacity of unidirectional quantum transduction increases with the transmission coefficient. Therefore we choose (Δ_1, Δ_2) that leads to the highest transmission rate T to achieve the information rates $(I_{\max}, 0)$ and $(0, I_{\max})$ on $\partial\mathsf{R}$. For $I_1 > 0$ and $I_2 > 0$, R corresponds to a continuous mapping $(N_1, N_2, \Delta_1, \Delta_2) \to (I_1, I_2)$. The boundary $\partial\mathsf{R}$ as extreme values of the mapping can be obtained by comparing two possible solutions. One solution is from the low-rank Jacobian condition $\mathrm{rank}(J) < 2$, where J is the 2×4 Jacobian matrix. The other solution is from the reflectionless condition with $R_k = 0$ and $N_k \to \infty$ where $k = 1$ or 2. We consider this solution separately since the Jacobian matrix may be undefined under the limit of $N_k \to \infty$. The reflectionless solution can be calculated analytically. For example, $R_1 = 0$ requires

$$\Delta_1 = \frac{\kappa_e - \kappa_i}{\kappa_e + \kappa_i} \Delta_2, \quad \Delta_2 = \sqrt{\frac{(\kappa_e + \kappa_i)(4g^2 - \kappa_e^2 + \kappa_i^2)}{4(\kappa_e - \kappa_i)}}, \tag{15}$$

which leads to the achievable rates at $N_1 \to \infty$

$$\begin{aligned} I_1(N_2) &= \log_2 \frac{T}{1-T} - h\left(R_2 N_2 \frac{1+T}{2(1-T)} \right), \\ I_2(N_2) &= h(TN_2) - h[(1-T)N_2]. \end{aligned} \tag{16}$$

In practice, we expect an approximate reflectionless solution with $R_k \approx 0$ and finite N_k, due to input power constraints and uncertainties in controlling the reflection coefficients.

We calculate the time-sharing rate region $\tilde{\mathsf{R}}(\kappa_e)$ for several choices of κ_e at $g = 5$ and $\kappa_i = 1$ [Fig. 3(b)]. The boundary $\partial\tilde{\mathsf{R}}$ may be composed of one or more types of the protocols: reflectionless (red), low-rank Jacobian (green), and time-sharing (gray). For example, for $9.63 < \kappa_e < 9.68$ the boundary contains all three types of protocols [Fig. 3(b)ii] while for $\kappa_e > 11.28$ or $\kappa_e < 6.2$ the optimized protocol is time-shared unidirectional transduction. It is also worth mentioning that for $6.2 < \kappa_e < 11.28$ the transducers benefit from the simultaneous duplex transduction.

If both κ_e and detunings are tunable, it can be proved that the highest transmission rate T occurs when $R_1 = R_2 = 0$ (see SM [41]). Therefore the optimal duplex quantum transduction is achieved with the two-sided reflectionless condition at $\kappa_e = \sqrt{4g^2 + \kappa_i^2}$ and $\Delta_1 = \Delta_2 = 0$ [Fig. 3(b) iv]. In other words, $\tilde{\mathsf{R}}(\sqrt{4g^2 + \kappa_i^2})$ is the largest possible region in the sense that $\tilde{\mathsf{R}}(\kappa_e) \subseteq \tilde{\mathsf{R}}(\sqrt{4g^2 + \kappa_i^2})$ for any κ_e.

Frequency-integrated rate region.—A quantum transducer usually has a finite conversion bandwidth, which determines the range of signal frequencies that can be converted efficiently [57]. A larger bandwidth enables higher operation speed of the transducer, and is preferable

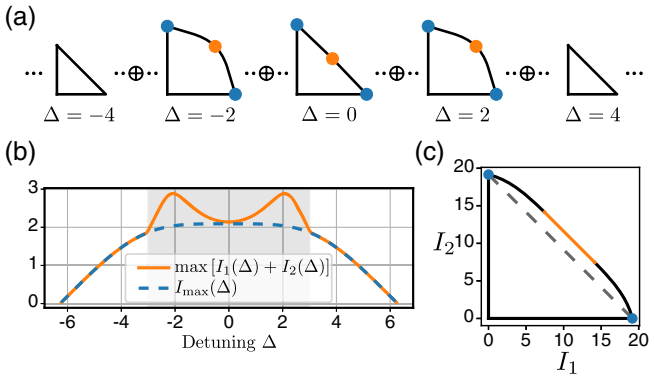

FIG. 4. (a) The time-sharing rate regions $\tilde{\mathsf{R}}(\Delta)$ for different signal frequencies. Here $g = 5, \kappa_e = 9, \kappa_i = 1$ are fixed. (b) Comparing the maximal $I_1(\Delta) + I_2(\Delta)$ with the quantum capacity $I_{\max}(\Delta)$. (c) Frequency-integrated rate region $\tilde{\mathsf{R}}_{\text{tot}}$ over all regions $\tilde{\mathsf{R}}(\Delta)$ in (a).

in the presence of decoherence. Within the bandwidth, quantum signals at multiple frequencies can be transduced independently with frequency-dependent conversion efficiencies.

We can perform duplex quantum transduction in parallel for various signal frequencies, and the frequency-dependent scattering matrices result in distinct achievable rate regions that vary with frequency. Let $\omega_2 = \omega_p + \omega_1$ for the transducer model Eq. (11); the signal detuning in the rotating frame becomes $\Delta_1 = \Delta_2 \equiv \Delta$, and the frequency-dependent rate region is $\mathsf{R}(\Delta) \equiv \{[I_1(\Delta), I_2(\Delta)] | \forall (N_1, N_2)\}$. We plot the time-sharing rate regions $\tilde{\mathsf{R}}(\Delta)$ for multiple Δ [Fig. 4(a)], and compare $\max[I_1(\Delta) + I_2(\Delta)]$ with the quantum capacity $I_{\max}(\Delta)$ [Fig. 4(b)]. For Δ within the gray shaded region, simultaneous duplex transduction is advantageous, while outside this region time-shared unidirectional transduction is the optimal protocol.

To obtain the total achievable rate region, we sum the contributions from the individual rate regions at each signal frequency [Fig. 4(a)]. The frequency-integrated rate region for time-shared duplex transduction is defined as

$$\tilde{\mathsf{R}}_{\text{tot}} \equiv \int^{\oplus} \tilde{\mathsf{R}}(\omega) \mathrm{d}\omega \approx \delta(\cdots \oplus \tilde{\mathsf{R}}(\omega_{j-1}) \oplus \tilde{\mathsf{R}}(\omega_j) \oplus \tilde{\mathsf{R}}(\omega_{j+1}) \oplus \cdots), \quad (17)$$

where $\{\omega_j\}$ is a set of evenly spaced frequencies with a frequency spacing δ, and $\mathsf{A} \oplus \mathsf{B} \equiv \{\boldsymbol{a} + \boldsymbol{b} | \boldsymbol{a} \in \mathsf{A}, \boldsymbol{b} \in \mathsf{B}\}$ is the Minkowski sum [58] of two sets A and B. For general sets the complexity of the Minkowski sum is $O(|A||B|)$, while for convex sets A and B in $\mathbb{R}^2$ the complexity is $O(|\partial A| + |\partial B|)$ [58]. Therefore numerical evaluation of $\tilde{\mathsf{R}}_{\text{tot}}$ is efficient since $\tilde{\mathsf{R}}$ is convex in $\mathbb{R}^2$.

We calculate the Minkowski sum of all rate regions $\tilde{\mathsf{R}}(\Delta)$ in Fig. 4(a), and the resulting frequency-integrated rate region $\tilde{\mathsf{R}}_{\text{tot}}$ is shown in Fig. 4(c). The boundary $\partial\tilde{\mathsf{R}}_{\text{tot}}$ can be achieved with frequency dependent protocols. For example, to realize the orange part of $\partial\tilde{\mathsf{R}}_{\text{tot}}$ with a slope of -1, we choose the simultaneous duplex transduction protocol that maximizes $I_1(\Delta) + I_2(\Delta)$ [Fig. 4(a) orange dots] for signal detuning Δ within the gray shaded region in Fig. 4(b). For other Δ, we perform the time-shared unidirectional transduction. Benefiting from simultaneous duplex transduction, the frequency-integrated rate region outperforms the time-shared unidirectional transduction [Fig. 4(c), gray dashed line].

Discussion.—We proposed the (time-sharing) rate region to quantify the performance of duplex quantum transduction and studied optimized protocols for a two-mode quantum transducer. Unlike unidirectional quantum transduction, duplex quantum transduction is influenced by the reflection coefficients, and we explored how the reflectionless condition can be related to the optimal duplex quantum transduction. Furthermore, we incorporated the finite bandwidth of the transducer and introduced the frequency-integrated rate region. In future works, it would be interesting to consider non-Gaussian encodings (see SM [41]), as well as other approaches to quantum transduction such as adaptive control [23], shared entanglement [52–54], and interference-based methods [55,56]. Our method can also be extended to analyze the performance of multiplex quantum hardware with more than two quantum channels, such as characterizing the performance of a 3-port quantum circulator with a three-dimensional rate region. Exploring alternative performance metrics [59] for duplex quantum transduction may provide further insights.

We thank Amir Safavi-Naeini, Cheng Guo, Chiao-Hsuan Wang, Mark M. Wilde, and Siddhartha Das for helpful discussions. We acknowledge support from the ARO (W911NF-23-1-0077), ARO MURI (W911NF-21-1-0325), AFOSR MURI (FA9550-19-1-0399, FA9550-21-1-0209), AFRL (FA8649-21-P-0781), NSF (OMA-1936118, ERC-1941583, OMA-2137642), NTT Research, and the Packard Foundation (2020-71479). L. J. acknowledges the support from the Marshall and Arlene Bennett Family Research Program. This material is based upon work supported by the U.S. Department of Energy, Office of Science, National Quantum Information Science Research Centers.

*zhaoyou@uchicago.edu
†liangjiang@uchicago.edu

[1] H. J. Kimble, Nature (London) **453**, 1023 (2008).
[2] N. J. Lambert, A. Rueda, F. Sedlmeir, and H. G. L. Schwefel, Adv. Quantum Technol. **3**, 1900077 (2020).
[3] X. Han, W. Fu, C.-L. Zou, L. Jiang, and H. X. Tang, Optica **8**, 1050 (2021).

[4] R. W. Andrews, R. W. Peterson, T. P. Purdy, K. Cicak, R. W. Simmonds, C. A. Regal, and K. W. Lehnert, Nat. Phys. **10**, 321 (2014).

[5] A. Vainsencher, K. J. Satzinger, G. A. Peairs, and A. N. Cleland, Appl. Phys. Lett. **109**, 033107 (2016).

[6] L. Fan, C.-L. Zou, R. Cheng, X. Guo, X. Han, Z. Gong, S. Wang, and H. X. Tang, Sci. Adv. **4**, eaar4994 (2018).

[7] A. Rueda, W. Hease, S. Barzanjeh, and J. M. Fink, npj Quantum Inf. **5**, 108 (2019).

[8] W. Jiang, C. J. Sarabalis, Y. D. Dahmani, R. N. Patel, F. M. Mayor, T. P. McKenna, R. Van Laer, and A. H. Safavi-Naeini, Nat. Commun. **11**, 1166 (2020).

[9] M. Mirhosseini, A. Sipahigil, M. Kalaee, and O. Painter, Nature (London) **588**, 599 (2020).

[10] T. P. McKenna, J. D. Witmer, R. N. Patel, W. Jiang, R. V. Laer, P. Arrangoiz-Arriola, E. A. Wollack, J. F. Herrmann, and A. H. Safavi-Naeini, Optica **7**, 1737 (2020).

[11] Y. Xu, A. A. Sayem, L. Fan, C.-L. Zou, S. Wang, R. Cheng, W. Fu, L. Yang, M. Xu, and H. X. Tang, Nat. Commun. **12**, 4453 (2021).

[12] H.-T. Tu, K.-Y. Liao, Z.-X. Zhang, X.-H. Liu, S.-Y. Zheng, S.-Z. Yang, X.-D. Zhang, H. Yan, and S.-L. Zhu, Nat. Photonics **16**, 291 (2022).

[13] Z. Shen, G.-T. Xu, M. Zhang, Y.-L. Zhang, Y. Wang, C.-Z. Chai, C.-L. Zou, G.-C. Guo, and C.-H. Dong, Phys. Rev. Lett. **129**, 243601 (2022).

[14] M. Tsang, Phys. Rev. A **81**, 063837 (2010).

[15] M. Aspelmeyer, T. J. Kippenberg, and F. Marquardt, Rev. Mod. Phys. **86**, 1391 (2014).

[16] K. Stannigel, P. Rabl, A. S. Sørensen, P. Zoller, and M. D. Lukin, Phys. Rev. Lett. **105**, 220501 (2010).

[17] A. H. Safavi-Naeini and O. Painter, New J. Phys. **13**, 013017 (2011).

[18] J. T. Hill, A. H. Safavi-Naeini, J. Chan, and O. Painter, Nat. Commun. **3**, 1196 (2012).

[19] T. A. Palomaki, J. W. Harlow, J. D. Teufel, R. W. Simmonds, and K. W. Lehnert, Nature (London) **495**, 210 (2013).

[20] F. Lecocq, J. B. Clark, R. W. Simmonds, J. Aumentado, and J. D. Teufel, Phys. Rev. Lett. **116**, 043601 (2016).

[21] X. Zhang, C.-L. Zou, L. Jiang, and H. X. Tang, Phys. Rev. Lett. **113**, 156401 (2014).

[22] Y. Tabuchi, S. Ishino, A. Noguchi, T. Ishikawa, R. Yamazaki, K. Usami, and Y. Nakamura, Science **349**, 405 (2015).

[23] M. Zhang, C.-L. Zou, and L. Jiang, Phys. Rev. Lett. **120**, 020502 (2018).

[24] C.-H. Wang, F. Li, and L. Jiang, Nat. Commun. **13**, 6698 (2022).

[25] Previous works on "bidirectional conversion" [4,5,8,11] measure the two unidirectional transduction channels separately on a single device, while the duplex quantum transduction we consider here is more general.

[26] O. Fawzi, P. Hayden, I. Savov, P. Sen, and M. M. Wilde, IEEE Trans. Inf. Theory **58**, 3670 (2012).

[27] P. Sen, in *2012 IEEE International Symposium on Information Theory Proceedings* (2012), pp. 736–740, 10.1109/ISIT.2012.6284656.

[28] S. Das, S. Bäuml, M. Winczewski, and K. Horodecki, Phys. Rev. X **11**, 041016 (2021).

[29] C. Bennett, A. Harrow, D. Leung, and J. Smolin, IEEE Trans. Inf. Theory **49**, 1895 (2003).

[30] A. M. Childs, D. W. Leung, and H.-K. Lo, Int. J. Quantum. Inform. **04**, 63 (2006).

[31] H. Shi, M.-H. Hsieh, S. Guha, Z. Zhang, and Q. Zhuang, npj Quantum Inf. **7**, 74 (2021).

[32] M. Pant, H. Krovi, D. Towsley, L. Tassiulas, L. Jiang, P. Basu, D. Englund, and S. Guha, npj Quantum Inf. **5**, 25 (2019).

[33] S. Shi and C. Qian, in *Proceedings of the Annual Conference of the ACM Special Interest Group on Data Communication on the Applications, Technologies, Architectures, and Protocols for Computer Communication*, SIGCOMM '20 (Association for Computing Machinery, New York, 2020), pp. 62–75.

[34] G. Vardoyan, S. Guha, P. Nain, and D. Towsley, ACM Sigmetrics Perform. Eval. Rev. **48**, 45 (2021).

[35] W. Dai, A. Rinaldi, and D. Towsley, in *2022 IEEE International Conference on Quantum Computing and Engineering (QCE)* (2022), pp. 389–399, 10.1109/QCE53715.2022.00060.

[36] M. M. Wilde, *Quantum Information Theory* (Cambridge University Press, Cambridge, England, 2013).

[37] B. Schumacher and M. A. Nielsen, Phys. Rev. A **54**, 2629 (1996).

[38] S. Lloyd, Phys. Rev. A **55**, 1613 (1997).

[39] I. Devetak, IEEE Trans. Inf. Theory **51**, 44 (2005).

[40] C. Weedbrook, S. Pirandola, R. García-Patrón, N. J. Cerf, T. C. Ralph, J. H. Shapiro, and S. Lloyd, Rev. Mod. Phys. **84**, 621 (2012).

[41] See Supplemental Material at http://link.aps.org/supplemental/10.1103/PhysRevLett.131.220802, which includes Refs. [42–47], for derivations of the achievable rates, other settings of duplex quantum transduction, optimality of two-sided reflectionless condition, asymmetric loss rates and non-Gaussian encodings.

[42] C. H. Bennett, D. P. DiVincenzo, and J. A. Smolin, Phys. Rev. Lett. **78**, 3217 (1997).

[43] R. García-Patrón, S. Pirandola, S. Lloyd, and J. H. Shapiro, Phys. Rev. Lett. **102**, 210501 (2009).

[44] S. Pirandola, R. Laurenza, C. Ottaviani, and L. Banchi, Nat. Commun. **8**, 15043 (2017).

[45] S. Bäuml, S. Das, and M. M. Wilde, Phys. Rev. Lett. **121**, 250504 (2018).

[46] S. Das, S. Bäuml, and M. M. Wilde, Phys. Rev. A **101**, 012344 (2020).

[47] D. Ding, S. Khatri, Y. Quek, P. W. Shor, X. Wang, and M. M. Wilde, IEEE Trans. Inf. Theory **69**, 3034 (2023).

[48] A. S. Holevo and R. F. Werner, Phys. Rev. A **63**, 032312 (2001).

[49] M. Rosati, A. Mari, and V. Giovannetti, Nat. Commun. **9**, 4339 (2018).

[50] K. Sharma, M. M. Wilde, S. Adhikari, and M. Takeoka, New J. Phys. **20**, 063025 (2018).

[51] K. Noh, V. V. Albert, and L. Jiang, IEEE Trans. Inf. Theory **65**, 2563 (2019).

[52] C. Zhong, Z. Wang, C. Zou, M. Zhang, X. Han, W. Fu, M. Xu, S. Shankar, M. H. Devoret, H. X. Tang, and L. Jiang, Phys. Rev. Lett. **124**, 010511 (2020).

[53] C. Zhong, X. Han, H. X. Tang, and L. Jiang, Phys. Rev. A **101**, 032345 (2020).
[54] J. Wu, C. Cui, L. Fan, and Q. Zhuang, Phys. Rev. Appl. **16**, 064044 (2021).
[55] H.-K. Lau and A. A. Clerk, npj Quantum Inf. **5**, 31 (2019).
[56] M. Zhang, S. Chowdhury, and L. Jiang, npj Quantum Inf. **8**, 71 (2022).
[57] E. Zeuthen, A. Schliesser, A. S. Sørensen, and J. M. Taylor, Quantum Sci. Technol. **5**, 034009 (2020).
[58] M. De Berg, O. Cheong, M. Van Kreveld, and M. Overmars, *Computational Geometry: Algorithms and Applications* (Springer, Berlin, Heidelberg, 2008).
[59] A. U. Siddiqui and M. M. Wilde, arxiv:2010.07905.